Suppression of pair creation due to a steady magnetic field

W. Su,[1] M. Jiang,[2] Z. Q. Lv,[1] Y. J. Li,[1] Z. M. Sheng,[2] R. Grobe,[3,4] and Q. Su[4]

[1]*State Key Laboratory for GeoMechanics and Deep Underground Engineering, China University of Mining and Technology, Beijing 100083, China*

[2]*Beijing National Laboratory for Condensed Matter Physics, Institute of Physics, Chinese Academy of Sciences, Beijing 100190, China*

[3]*Max-Planck-Institut für Kernphysik, Saupfercheckweg 1, D-69117 Heidelberg, Germany*

[4]*Intense Laser Physics Theory Unit and Department of Physics, Illinois State University, Normal, Illinois 61790-4560, USA*

(Received 17 April 2012; published 26 July 2012)

We investigate the electron-positron pair creation process in a supercritical static electric field in the presence of a static magnetic field that is perpendicular. If both fields vary spatially in one direction the dynamics can be reduced to a set of one-dimensional systems. Using a generalized computational quantum field theoretical procedure, we calculate the time dependence of the spatial density for the created electrons. In the presence of the magnetic field, a significant amount of suppression of pair creation is observed in the simulations and confirmed by an analytical analysis for the limits of short-range fields and long interaction times. This suppression might be interpreted in terms of Pauli blocking by the electron during its return to the creation region as it performs a cyclotronlike motion in the magnetic field.

DOI: 10.1103/PhysRevA.86.013422 PACS number(s): 34.50.Rk, 03.65.−w

I. INTRODUCTION

The electron-positron (e^+-e^-) pair production process triggered by an external field has a long history pioneered by the discovery of the Klein paradox [1] and then further investigated by Sauter [2]. It was found that there is a nonvanishing transmission of an incoming electron as it scatters off a repulsive potential step whose height exceeds twice the rest mass energy of the electron. Contradictory arguments can be constructed in the theoretical framework of a single-particle theory, but this paradox can be resolved if one treats it as a problem in quantum field theory in which, in addition to the incoming electron, the creation of particles from the vacuum is also included. It turns out that the result of the Klein transmission can help us to compute the long-time behavior of the pair creation rate. In 1951, Schwinger [3] proposed the proper time method to describe the long-time behavior of e^+-e^- pair production process in a static and spatially uniform electric field. As a result, particle creation in a classical electric field is often referred to as the Schwinger mechanism. The typical electric field strength for spontaneous pair production requires an extraordinarily strong electric field, which corresponds to $E_{\rm cr} = 1.3 \times 10^{16}$ V/cm. Although the problem of creating such an ultraintense field under laboratory conditions remains presently unsolved, the study is important as it urges us to go beyond the scope of perturbation theory to probe the domain of ultraintense field-vacuum interactions.

The e^+-e^- production in a classical electric field has been extensively studied theoretically since Schwinger. Hansen and Ravndal [4] and Holstein [5,6] used the Sauter potential to extend Schwinger's work to compute the long-time pair creation behavior due to spatially inhomogeneous but time-independent electric fields. Analytical and numerical estimations of the leading-order pair-creation rate in spatially inhomogeneous or time-dependent electric field were also obtained using the instanton approximation of the world line path-integral formulation of quantum field theory [7–10].

The pair production in combined electromagnetic (EM) fields has also been studied. According to textbooks [11], the creation rate is eventually related to the solutions of the Dirac equation in the external fields. Exact solutions exist only for very simple field configurations such as plane EM waves and spatially uniform and temporally steady electric and magnetic fields [12]. For uniform static electric and magnetic fields with arbitrary directions, the result is similar to the case where the **E** and **B** fields are parallel to each other. Here the effective electric and magnetic field strengths are given by $\{[\sqrt{({F_1}^2+{F_2}^2)}+F_1]/2\}^{1/2}$ and $\{[\sqrt{({F_1}^2+{F_2}^2)}-F_1]/2\}^{1/2}$, respectively, where the Lorentz invariants are defined as $F_1 = \mathbf{E}^2 - \mathbf{B}^2$ and $F_2 = 2\mathbf{E}\cdot\mathbf{B}$ [13,14]. When the magnetic field is perpendicular to the electric field, $F_2 = 0$, then an increasing magnetic field reduces the effective electric field strength leading naturally to a lower pair creation rate. Thus, this kind of magnetic field suppresses the pair creation in the uniform and constant electric field. To mention another extreme case, both F_1 and F_2 can be equal to zero for a plane EM wave, such that no pairs are produced. The pair production in a strong time-dependent magnetic field [15] was calculated in the framework of adiabatic perturbation theory that is based on the Landau levels characteristic of a uniform magnetic field. For spatially inhomogeneous EM fields, such an energy level structure is not apparent. A direct calculation of the pair creation in inhomogeneous and time-dependent EM fields can provide us with further understanding of this nonperturbative mechanism.

Recently, due to the continued advancement of laser systems with extremely high power, the pair creation triggered solely by a laser has become a hot research topic. First laser-based experiments were carried out at SLAC [16] in 1997 and reported on the multiphoton pair creation in the collision of a relativistic electron with a strong laser beam. Theoretical calculations were based on a laser-dressed quantum electrodynamics [17]. Theoretical predictions were also made for the pair creation that involves the nucleus in the laser fields [18–24]. The creation process triggered solely by a laser

has the virtue of being free of any nuclear processes and can be studied more unambiguously on the theoretical level. Several works have generalized the Schwinger formula to include also the finite temporal extent of laser pulses [25,26]. The authors focused on the nonadiabatic correction to the temporal extent of the laser field and integrated the Schwinger formula over the creation region by employing a constant-field approximation locally. Other works examined catalysis mechanisms such as superposition of a strong low-frequency and a weak high-frequency laser field [27–29] and counterpropagating laser pulses [20,21,30], where magnetic fields are often neglected.

It is important to note that as the e^+–e^- production is not necessarily a spatially localized effect [9,31], the spatial nonuniformity of the laser beam can be neglected only when the creation region is much larger than the Compton length, $\hbar/(mc)$. The effect of the magnetic field component cannot be neglected in the upcoming x-ray free-electron laser facilities [32–34]. The magnetic field component for currently available laser pulse at the intensity of 10^{20} W/cm^2 is about 1 GG. The focused intensity for the planned ELI laser is expected to reach an intensity level of 10^{24} W/cm^2, with the magnetic field on the order of 100 GG. The experimentally measured quasistatic **B** field has already reached 300 MG at a laser intensity about 10^{19} W/cm^2 [35,36]. The supercritical magnetic field strength corresponds to 4.4×10^{13} G $= 4.4 \times 10^9$ T, which is reached when laser electric field reaches the $E_{\rm cr}$ value.

This work attempts to build a general framework to calculate the pair creation process in EM fields of both time-dependent and spatially inhomogeneous field configurations. It is our intention to make use of a computational method to study systematically various field configurations involving the magnetic field. This method allows us to calculate the impact of the the magnetic field on the temporal and spatial characteristics of the process. In particular, we make a direct calculation of the e^+–e^- production process for inhomogeneous static fields where the electric field and magnetic field are perpendicular to each other and their magnitude varies in one direction. The approach is based on a numerical code used to solve the time-dependent Dirac equation in arbitrary dimensions. The pair production is often viewed as the result of a field-induced transition between states of negative and positive energy. Prior studies based on this code have already provided some insights into various conceptual problems in quantum field theory [37–40]. In this work, the method is extended to accommodate for the presence of the magnetic field and also higher spatial dimensions. The long-time behavior of e^+–e^- production process can be related to one-particle quantum-mechanical tunneling. One-particle tunneling in an extremely narrow EM field can also be solved analytically. In another limiting case where the EM fields remain uniform over a large range, the numerical results reproduce the modified Schwinger pair-production rate.

The paper is organized as follows. In Sec. II, we describe a quantum field theory (QFT) algorithm to calculate the pair creation process in arbitrary EM fields. In Sec. III, we propose a model for which we calculate the pair creation with temporal and spatial resolution for the special case in which the magnitude of both fields varies in one direction. We apply our QFT framework to the static and mutually perpendicular electric and magnetic fields. In Sec. IV we compare the spatial distributions of the single-particle wave function for two-dimensional (2D) and 1D systems. In Sec. V the spatial densities are calculated and analyzed for different transverse momentum values. In Sec. VI we analyze the long-time behavior of the pair creation rate and relate it to single-particle tunneling between positive and negative energy states. The two extreme cases of spatially narrow and wide fields are studied analytically. In Sec. VII we discuss some interesting but not very well understood questions and outline further research directions.

II. QUANTUM FIELD THEORETICAL DESCRIPTION OF PAIR CREATION IN ARBITRARY EXTERNAL FIELDS

The pair creation in classical EM fields needs to be studied within the framework of QFT [41]. Former works have focused on pair creation in electric fields [37,40], where the Dirac equation is second quantized within a Hilbert space of interaction-free basis states. In intuitive terms, the field is switched on suddenly at $t = 0$ and switched off at the time we make the measurement. The switch-on and -off causes no difficulty for the electric field in the V gauge (scalar potential) as no other improper fields are created. For the case when a magnetic field is present, however, the corresponding vector potential **A** becomes unavoidable and needs to be included. The switch-on and switch-off process would lead to an—in principle—infinite amount of electric field that could obscure the underlying physical mechanisms.

In this section we try to formulate a general framework to calculate the pair creation process in classical EM fields. In order to unambiguously detect the created pairs we consider the scalar potential free Dirac Hamiltonian (from now on we use atomic units)

$$h_0(t) = c\alpha \cdot (\mathbf{p} + \mathbf{A}/c) + \beta c^2. \tag{2.1}$$

As the Hamiltonian $h_0(t)$ is Hermitian at every instant of time t, we can assume that there exists an orthonormal and complete basis set of (instantaneous) eigenstates satisfying

$$h_0(t)\psi_{\mathcal{P}}(\mathbf{x}) = E_{\mathcal{P}}(t)\psi_{\mathcal{P}}(\mathbf{x}), \tag{2.2a}$$

$$h_0(t)\psi_{\mathcal{N}}(\mathbf{x}) = E_{\mathcal{N}}(t)\psi_{\mathcal{N}}(\mathbf{x}). \tag{2.2b}$$

The subscript $\mathcal{P}(\mathcal{N})$ denotes positive (negative) energy eigenstates. Note that $E_{\mathcal{P}} > 0$ and $E_{\mathcal{N}} < 0$ and that a gap exists between positive and negative energy levels. In the case of a pure electric field, this claim is proved explicitly in Appendix A. The main reason for excluding a scalar potential is that for the case of $V > 2c^2$, it could be difficult to distinguish between positive and negative energy states. Note that $\psi_{\mathcal{P}}$ and $\psi_{\mathcal{N}}$ are only instant eigenfunctions of $h_0(t)$; they do not evolve with time as they are not solutions to the time-dependent Dirac equation. The orthonormal and complete relations read

$$\int dx\ \psi_U^\dagger(\mathbf{x})\psi_V(\mathbf{x}) = \delta_{UV}, \tag{2.3a}$$

$$\sum_U \psi_U(\mathbf{x})\psi_U^\dagger(\mathbf{x}') = \delta(\mathbf{x} - \mathbf{x}'), \tag{2.3b}$$

where U, $V = \mathcal{P}$ or $\mathcal{N}$, and we do not denote the spinors explicitly here. The field operator can be expanded as

$$\hat{\Psi}(\mathbf{x},t) = \sum_{\mathcal{P}} \hat{B}_{\mathcal{P}}(t)\psi_{\mathcal{P}}(\mathbf{x}) + \sum_{\mathcal{N}} \hat{D}^{\dagger}_{\mathcal{N}}(t)\psi_{\mathcal{N}}(\mathbf{x}), \quad (2.4)$$

where $\hat{B}_{\mathcal{P}}(t)$ and $\hat{D}^{\dagger}_{\mathcal{N}}(t)$ are the annihilation and creation operators for positive-energy states $\psi_{\mathcal{P}}(\mathbf{x})$ and negative-energy states $\psi_{\mathcal{N}}(\mathbf{x})$ at the instant t. They satisfy the anti-commutator algebra: $[\hat{B}_{\mathcal{P}1}(t), \hat{B}_{\mathcal{P}2}(t)]_+ = 0$, $[\hat{B}_{\mathcal{P}1}(t), \hat{B}^{\dagger}_{\mathcal{P}2}(t)]_+ = \delta_{\mathcal{P}1\mathcal{P}2}$, and similar relations hold for $\hat{D}$.

Independently, integrating the single-particle Dirac equation $i\,\partial\phi/\partial t = h(t)\,\phi$, with the full Hamiltonian including the influence of the combined **E** and **B** fields $h(t) \equiv h_0(t) + V(t)$, forward in time from a complete set of eigenmodes $\varphi_p(\mathbf{x}, t_0)$ and $\varphi_n(\mathbf{x}, t_0)$ at an initial moment t_0 gives another set of solutions $\varphi_p(\mathbf{x}, t)$ and $\varphi_n(\mathbf{x}, t)$ at time t. Here $\varphi_p(\mathbf{x}, t_0)$ and $\varphi_n(\mathbf{x}, t_0)$ denote the positive and negative states at t_0, with $\varphi_p(\mathbf{x}, t_0) \equiv \psi_{\mathcal{P}}(\mathbf{x})$ and $\varphi_n(\mathbf{x}, t_0) \equiv \psi_{\mathcal{N}}(\mathbf{x})$. Since $h(t)$ is Hermitian, $\varphi_p(x, t)$ and $\varphi_n(x, t)$ form another complete, orthonormal basis set at every instant of time t:

$$\int dx\ \phi^{\dagger}_u(\mathbf{x},t)\,\phi_v(\mathbf{x},t) = \delta_{uv}, \quad (2.5a)$$

$$\sum_u \phi_u(\mathbf{x},t)\,\phi^{\dagger}_u(\mathbf{x}',t) = \delta(\mathbf{x}-\mathbf{x}'). \quad (2.5b)$$

Here $u, v = p, n$. The orthogonality and completeness relation can be proven by showing that the scalar product remains time independent, $\frac{d}{dt}\int dx\ \phi^{\dagger}_u\phi_v = \int dx(\dot{\phi}^{\dagger}_u\phi_v + \phi^{\dagger}_u\dot{\phi}_v) = \int dx\ [(-ih\phi_u)^{\dagger}\phi_v + \phi^{\dagger}_u(-ih\phi_v)] = i\int dx(\phi^{\dagger}_u h^{\dagger}\phi_v - \phi^{\dagger}_u h\phi_v) = 0$, and similarly, $\frac{d}{dt}(\sum_u \phi_u\phi^{\dagger}_u)^{\dagger} = 0$. Therefore, the field operator can also be expanded as $\hat{\Psi}(\mathbf{x},t) = \sum_u \hat{b}_u\,\phi_u(\mathbf{x},t)$. Operator $\hat{b}_u$ is time independent if $\phi_u(\mathbf{x},t)$ satisfies the time-dependent Dirac equation. To see this we note that $\hat{\Psi}$ satisfies the Dirac equation, so $0 = (\frac{\partial}{\partial t} + ih)\hat{\Psi} = \sum_u \dot{\hat{b}}_u(t)\phi_u(\mathbf{x},t) - i\sum_u \hat{b}_u(t)(i\frac{\partial}{\partial t} - h)\phi_u(\mathbf{x},t) = \sum_u \dot{\hat{b}}_u(t)\phi_u(\mathbf{x},t)$. The projection with a function $\phi_u(\mathbf{x},t)$ at time t shows that the operators $\hat{b}_u$ are time independent. Using this argument we can expand the field operator as

$$\hat{\Psi}(\mathbf{x},t) = \sum_p \hat{b}_p\phi_p(\mathbf{x},t) + \sum_n \hat{d}^{\dagger}_n\phi_n(\mathbf{x},t), \quad (2.6)$$

where $\hat{b}_p$ and $\hat{d}^{\dagger}_n$ are defined as $\hat{b}_p = \hat{b}_p(t_0)$ and $\hat{d}^{\dagger}_n = \hat{b}_n(t_0)$. They are the annihilation and creation operators for the positive energy states $\phi_p(x,t_0)$ and the negative energy states $\phi_n(x,t_0)$ at the initial time t_0. They satisfy the anti-commutators $[\hat{b}_{p1},\hat{b}_{p2}]_+ = 0$ and $[\hat{b}_{p1},\hat{b}^{\dagger}_{p2}]_+ = \delta_{p1,\,p2}$, which also hold for $\hat{d}$.

Comparing Eqs. (2.4) and (2.6) one can show that the operators in Eq. (2.4) evolve in time according to

$$\hat{B}_{\mathcal{P}}(t) = \sum_p \hat{b}_p\ U_{\mathcal{P},p}(t) + \sum_n \hat{d}^{\dagger}_n\ U_{\mathcal{P},n}(t), \quad (2.7a)$$

$$\hat{D}^{\dagger}_{\mathcal{N}}(t) = \sum_p \hat{b}_p\ U_{\mathcal{N},p}(t) + \sum_n \hat{d}^{\dagger}_n\ U_{\mathcal{N},n}(t). \quad (2.7b)$$

Here we define the matrix element $U_{\alpha,\beta}(t) = \langle\psi_\alpha|\phi_\beta(t)\rangle$ with $\alpha = \mathcal{P}$ or $\mathcal{N}$ and $\beta = p$ or n. With these relations and an initial state at time t_0, we can define quantum field observations at any time t. For example, if the system is initially in the vacuum state $||0\rangle$ state at time t_0, with $\hat{b}_p||0\rangle = \hat{d}_n||0\rangle = 0$, we can define the average number of the electrons at t as

$$N(t) = \langle 0\|\sum_{\mathcal{P}} \hat{B}^{\dagger}_{\mathcal{P}}(t)\hat{B}_{\mathcal{P}}(t)\|0\rangle = \sum_{\mathcal{P}}\sum_n |U_{\mathcal{P},n}(t)|^2. \quad (2.8)$$

Other quantities such as the spatial density can also be computed from the operators in Eq. (2.8) and will be derived in the following sections.

III. APPLICATION TO PAIR CREATION IN STEADY ELECTRIC AND MAGNETIC FIELDS FOR A MODEL SYSTEM

For the case of a static and uniform electric field parallel to a static and uniform magnetic field we refer to the work of [12,14]. In this work we take the case of a time-independent magnetic field (assumed to point in the z direction) and a time-independent electric field (pointing in the x direction). This field configuration can be described by a vector potential **A** only or (as we have done) by **A** for the magnetic field and a scalar potential V for the electric field. The later description requires V to be switched on at $t = 0$ and switched off at the time one makes the measurement. These two gauge choices lead, of course, to the same result but the later one largely simplifies the numerical computation because for a constant vector potential Eqs. (2.2) become time independent.

In this work we assume for each simulation that the spatially localized magnetic field is temporally constant and therefore acts as a constant background at all times. The initial state is the QFT vacuum state associated with this magnetic field. We could equivalently assume that the vacuum is initially in the field-free state and the magnetic field (via the vector potential **A**) is turned on adiabatically from $t = -\infty$ to its full strength at $t = 0$. If the magnetic field were turned on nonadiabatically and too rapidly, the associated electric field by itself could possibly lead to a small amount of pair creation, which, however, is not the focus of our attention here. The true interaction (with $\mathbf{A} = \text{const.}$) begins at $t = 0$, when the strong electric field (via the scalar potential V) is turned on, and it is completed after V is turned off. The observables are computed then by projecting on the corresponding states in the presence of the magnetic background. If the electric field were turned on or off too abruptly, this rapid temporal change by itself could induce the creation of pairs, even if the amplitude of the electric field is still subcritical. We also illustrate below the dynamical manifestation of this turn-on effect.

In our model (where $\mathbf{E}\cdot\mathbf{B} = 0$) the electron's motion is confined to the x-y coordinate plane and executes a 2D motion if initially there is no velocity in the z direction. We consider further that the 2D Dirac Hamiltonian under investigation contains vector and scalar potentials **A** and V that only vary in the x direction. This corresponds to **E** and **B** fields that also vary only in the x direction. In such a field configuration, the 2D problem can be reduced to a set of effective 1D dynamics and therefore avoids an exceeding amount of computations. A similar kind of consideration has been introduced to classical problems. For example, this simplification is often exploited in particle-in-cell simulations in plasma physics [42,43], where the 3D evolution of particles accumulates to a 1D statistical

distribution:

$$h(x) \equiv h_0 + V(x) \equiv c\alpha_x\ \hat{p}_x + c\alpha_y\ \hat{p}_y + \alpha_y\ A_y(x) + \beta c^2 + V(x). \quad (3.1)$$

As the commutator $[\hat{p}_y,h]$ vanishes, the momentum p_y is a conserved quantity. For particle detection we consider the scalar-potential-free situation first. The basis in Hilbert space of h_0 can be chosen as $\psi_\alpha^{p_y}(x,y) = \chi_\alpha^{p_y}(x)e^{ip_y y}/\sqrt{2\pi}$, where $h_0^{p_y}\chi_\alpha^{p_y}(x) = E_\alpha^{p_y}\chi_\alpha^{p_y}(x)$ and $\alpha = \mathcal{P}$ or $\mathcal{N}$ while (the reduced h_0) $h_0^{p_y} \equiv c\alpha_x\hat{p}_x + c\alpha_y p_y + \alpha_y A_y(x) + \beta c^2$. Note that in the definition p_y has become a fixed number rather than an operator. The functions $\chi_\alpha^{p_y}(x)$ form a basis of $h_0^{p_y}$. Generally speaking, it is difficult to obtain an analytical expression for $\chi_\alpha^{p_y}(x)$ for arbitrary EM fields. However, with the help of the field-free states with a fixed momentum p_y along the y axis, they can be calculated numerically. The $\psi_\alpha^{p_y}(x,y)$ form an orthonormal and complete basis set for the Dirac Hamiltonian h_0 with

$$h_0\psi_\alpha^{p_y}(x,y) = h_0^{p_y}\chi_\alpha^{p_y}(x)e^{ip_y y}/\sqrt{2\pi} = E_\alpha^{p_y}\psi_\alpha^{p_y}(x,y). \quad (3.2)$$

To calculate the time evolution of $h(x)$ we start from the positive and negative energy eigenstates at initial time t_0 $\phi_p^{p_y}(x,y,t_0) = \zeta_p^{p_y}(x,t_0)e^{ip_y y}/\sqrt{2\pi}$ and $\phi_n^{p_y}(x,y,t_0) = \zeta_n^{p_y}(x,t_0)e^{ip_y y}/\sqrt{2\pi}$. The time evolution of this basis is given by the Dirac equation $i\partial\phi(x,y,t)/\partial t = h\ \phi(x,y,t)$. The time evolution can be factorized into $\phi_\beta^{p_y}(x,y,t) = \zeta_\beta^{p_y}(x,t)e^{ip_y y}/\sqrt{2\pi}$, where $\zeta(x,t)$ evolves as

$$i\partial\ \zeta_\beta^{p_y}(x,t)/\partial t = h^{p_y}\ \zeta_\beta^{p_y}(x,t), \quad (3.3)$$

while $h^{p_y} = h_0^{p_y} + V(x)$ and $\beta = n$ or p. Equation (3.3) and $\zeta_n^{p_y}(x,t_0)$ define an initial value problem which can be solved using the split-operator technique [44,45]. The field operator can be expanded as

$$\hat{\Psi}(x,y,t) = \sum_{\mathcal{P},\ p_y}\hat{B}_\mathcal{P}^{p_y}(t)\ \psi_\mathcal{P}^{p_y}(x,y) + \sum_{\mathcal{N},\ p_y}\hat{D}_\mathcal{N}^{p_y\ \dagger}(t)\ \ \psi_\mathcal{N}^{p_y}(x,y) = \frac{1}{\sqrt{L_y}}\sum_{p_y}e^{ip_y y} \times\left[\sum_\mathcal{P}\hat{B}_\mathcal{P}^{p_y}(t)\chi_\mathcal{P}^{p_y}(x) + \sum_\mathcal{N}\hat{D}_\mathcal{N}^{p_y\ \dagger}(t)\chi_\mathcal{N}^{p_y}(x)\right] \quad (3.4a)$$

or

$$\hat{\Psi}(x,y,t) = \sum_{p,\ p_y}\hat{b}_p^{p_y}\phi_p^{p_y}(x,y,t) + \sum_{n,\ p_y}\hat{d}_n^{p_y\ \dagger}\ \phi_n^{p_y}(x,y,t) = \frac{1}{\sqrt{L_y}}\sum_{p_y}e^{ip_y y} \times\left[\sum_p\hat{b}_p^{p_y}\ \zeta_p^{p_y}(x,t) + \sum_n\hat{d}_n^{p_y\ \dagger}\ \zeta_n^{p_y}(x,t)\right]. \quad (3.4b)$$

Here superscripts p_y in $\hat{B}_\mathcal{P}^{p_y}$, $\hat{b}_p^{p_y}$, $\hat{D}_\mathcal{N}^{p_y\dagger}$, and $\hat{d}_n^{p_y\dagger}$ denote annihilation or creation operators with fixed p_y, respectively. For our numerical calculations, we discretize p_y by introducing a numerical box with length L_y along the y axis. The creation and annihilation operators satisfy the algebra $[\hat{b}_{p_1}^{p_y},\hat{b}_{p_2}^{p'_y}]_+ = 0$ and $[\hat{b}_{p_1}^{p_y},\hat{b}_{p_2}^{p'_y\dagger}]_+ = \delta_{p_1\ p_2}\ \delta_{p_y\ p'_y}$, which also hold for $\hat{d}$, $\hat{B}$, and $\hat{D}$. The time-dependent operators $\hat{B}_\mathcal{P}^{p_y}(t)$ and $\hat{D}_\mathcal{N}^{p_y\ \dagger}(t)$ are given by

$$\hat{B}_\mathcal{P}^{p_y}(t) = \sum_p\hat{b}_p^{p_y}U_{\mathcal{P},n}^{p_y}(t) + \sum_n\hat{d}_n^{p_y\ \dagger}\ U_{\mathcal{P},n}^{p_y}(t), \quad (3.5a)$$

$$\hat{D}_\mathcal{N}^{p_y\ \dagger}(t) = \sum_p\hat{b}_p^{p_y}U_{\mathcal{N},p}^{p_y}(t) + \sum_n\hat{d}_n^{p_y\ \dagger}U_{\mathcal{N},n}^{p_y}(t). \quad (3.5b)$$

Here the matrix element is defined as $U_{\alpha,\beta}^{p_y}(t) = \langle\chi_\alpha^{p_y}|\zeta_\beta^{p_y}(t)\rangle$, while $\alpha = \mathcal{P}$ or $\mathcal{N}$ and $\beta = p$ or n.

For a system in the (magnetic field dressed) vacuum state $||0\rangle$ at t_0, the average electric density is

$$\rho_e(x,y,t) = \langle 0||\hat{\Psi}_e^\dagger(x,y,t)\hat{\Psi}_e(x,y,t)||0\rangle = \frac{1}{L_y}\langle 0||\left[\sum_{\mathcal{P},p_y}\hat{B}_\mathcal{P}^{p_y\ \dagger}(t)\ \hat{\chi}_\mathcal{P}^{p_y\ \dagger}(x)e^{ip_y y}\right] \times\left[\sum_{\mathcal{P}',p'_y}\hat{B}_{\mathcal{P}'}^{p'_y}(t)\chi_{\mathcal{P}'}^{p'_y}(x)e^{-ip'_y y}\right]||0\rangle = \frac{1}{L_y}\sum_{p_y,n}\left|\sum_\mathcal{P}U_{\mathcal{P},n}^{p_y}(t)\chi_\mathcal{P}^{p_y}(x)\right|^2. \quad (3.6)$$

Obviously, this result is y independent and we can integrate over y to remove the factor $1/L_y$. Integrating over x and y gives the average total amount of pair creation

$$N_e(t) = \sum_{\mathcal{P},\ p_y,n}\left|U_{\mathcal{P},n}^{p_y}(t)\right|^2. \quad (3.7)$$

The reduction of the 2D problem to a set of quasi-1D systems discussed above is applicable to more general configurations. For example, a 3D problem where the EM fields (time dependent or time independent) vary in the same spatial dimension can be treated with the same procedure. This simplification, however, not only largely reduces the amount of numerical computations (it currently still takes days of computing time), but it can also be relevant to other experimental conditions such as two counterpropagating laser pulses.

IV. SINGLE-PARTICLE DYNAMICS FOR MODEL 2D AND 1D SYSTEMS IN A STATIC B FIELD

With the considerations discussed in Sec. III we calculate a 2D system that varies in one spatial dimension. We will compare the exact 2D cyclotron motion in the x-y plane of an electron wave packet in a constant magnetic field and its marginal x-dependent density (obtained by integrating the density over y) with a 1D theory. To keep the comparison as illustrative as possible we investigate here the situation in which we approximate the 1D theory by only a single value of the external parameter p_y.

Figure 1 shows the comparison between 2D and 1D single-particle wave function evolutions for a Gaussian wave packet in a constant magnetic field. The gauge is chosen to

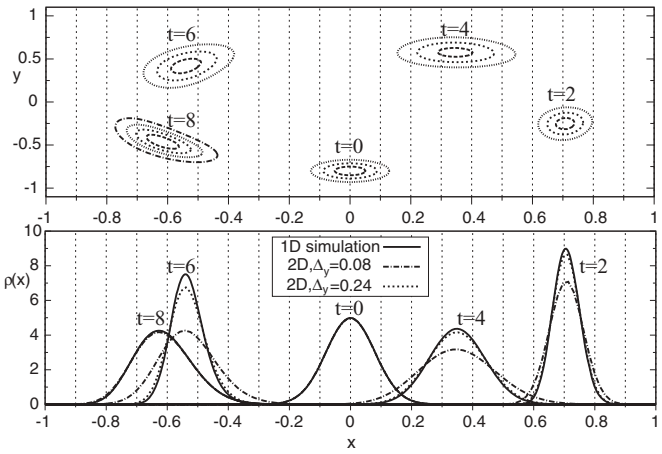

FIG. 1. Comparison between 2D (top) and 1D (bottom) evolutions of a Gaussian wave packet in a constant magnetic field along the z direction with $A_x = A_z = V = 0$, $A_y = B\,x$, and $\Delta_y = \Delta_x = 0.08$ a.u. For the 2D simulation (top) the y variable is integrated out, and the marginal x density is shown as the dot-dashed curve in the lower panel. In a second 2D simulation, $\Delta_y = 0.24$ a.u. is used, which produces x density indicated as the dashed curve. For the 1D simulation $p_y = 0$ is used and the evolution is the solid curve. Time t is labeled in units of 0.006 a.u. The wave packet has a cyclotron radius of 0.73 a.u. and a period of 0.057 a.u.

be $A_x = V = 0$, and $A_y = Bx$. In other words, the constant magnetic field is assumed to be along the z direction. For an illustration of the gauge equivalence between the choice of V and $\mathbf{A}$ fields, see Appendix A. We use $p_y = 0$ for the 1D simulation.

For the 2D simulation, the initial wave function is chosen as

$$\psi\,(x,y,t=0) = N_0 \begin{pmatrix} 1 \\ 0 \\ 0 \\ \frac{ck_0}{c^2+\sqrt{c^4+c^2k_0^2}} \end{pmatrix} \exp(ik_0x) \times \exp\left[-\frac{x^2}{(2\Delta_x)^2}\right] \exp\left[-\frac{(y-y_0)^2}{(2\Delta_y)^2}\right]. \quad (4.1a)$$

For the 1D simulation, the corresponding initial wave function is chosen as

$$\psi\,(x,t=0) = N_0 \begin{pmatrix} 1 \\ 0 \\ 0 \\ \frac{ck_0}{c^2+\sqrt{c^4+c^2k_0^2}} \end{pmatrix} \exp(ik_0x) \times \exp\left[-\frac{x^2}{(2\Delta_x)^2}\right], \quad (4.1b)$$

with $k_0 = 100$, N_0 are the corresponding normalization factors, and we set $B = c^2$. Equations (4.1) were chosen such that the marginal and 1D density are identical at $t = 0$ to allow for a better comparison.

The motion of the exact marginal density of this 2D wave packet is very well approximated by the effective 1D theory (based on a single value $p_y = 0$), if the initial transverse width Δ_y is chosen large enough. In this limit the momentum density is rather narrowly distributed around $p_y = 0$, and other p_y values, which would make our approximation (based here on $p_y = 0$) less valid, are not so important. Had we included all possible values of p_y the set of the 1D equations would, of course, be completely identical to the full 2D dynamics. This simplification is generally not possible when the **E** and **B** fields are parallel to each other when the dynamics is truly 3D. Our model system allows us to analyze the pair creation in great detail using realistic computation times. For the width $\Delta_y = 0.24$ the 2D motion (with the y motion integrated out) is already very close to the corresponding 1D evolution. For still larger width $\Delta_y > 0.5$ it becomes essentially indistinguishable from the 1D motion.

V. PAIR CREATION AND SPATIAL DENSITY IN COMBINED STATIC E AND B FIELDS

In this section we calculate the pair creation for time-independent but spatially inhomogeneous electric and magnetic fields. The electric field is represented by the corresponding scalar potential $V(x) = V_0[1 + \tanh(x/W)]/2$ and the magnetic field is given by vector potential components $A_y(x) = M[1 + \tanh(x/W)]/2$, and $A_x = A_z = 0$. These scalar and vector potentials correspond to an **E** field pointing in the x direction and a **B** field pointing in the z direction. Both fields vary along the x direction within a range of about $2W$ around $x = 0$. Note that since $E = -dV(x)/dx \sim V_0/(2W)$, at the peak around $x = 0$, and $B = dA_y(x)/dx \sim M/(2W)$, V and M can be expressed in units of c^2 and, for $W \sim 1/c$, E and B are given in units of c^3. We also see here that M is directly proportional to the B field. While spatial inhomogeneities make many standard theoretical approaches more difficult, they have the advantage that we can examine the dynamics also from a spatially resolved perspective. The system is initially in the QFT vacuum state $\|\,0\rangle$ in the magnetic field where V is switched off and the magnetic field is present. The overall pair creation is obtained by summing up all p_y contributions. Since our computations require us to scan through all values of p_y, it seems interesting to examine first how each individual p_y component contributes to the pair creation.

A. For momentum $p_y = 0$

The corresponding Hamiltonian for the special case of $p_y = 0$ simplifies to

$$h = c\alpha_x \hat{p}_x + \alpha_y A_y(x) + \beta c^2 + V(x). \quad (5.1)$$

The total number of created electron-positron pairs is illustrated in Fig. 2. The two curves labeled with $p_y = 0$ start from zero when the fields are turned on. Even though the two simulations differ by their magnetic field values, the number of created pairs for both is virtually identical within a time period that is close to $1/c^2 = 0.000\,05$. After this the curves turn into straight lines with constant slopes in the long-time limit. The slopes measured from Fig. 2 are 843.93 and 407.75 for the cases of $B = 0$ and $B \neq 0$ that corresponds to $M = 0.6c^2$, respectively. It is obvious that the presence of the magnetic field has reduced the pair creation rate by as much as a factor of 2 for $p_y = 0$. Note that the E field is supercritical, since $V_0 = 2.5c^2$ and $E \sim V_0/(2W) = 2.5c^2/(0.2/c) = 12.5c^3$. The magnetic field was $B \sim M/(2W) = 0.6c^2/(0.2/c) = 3c^3$.

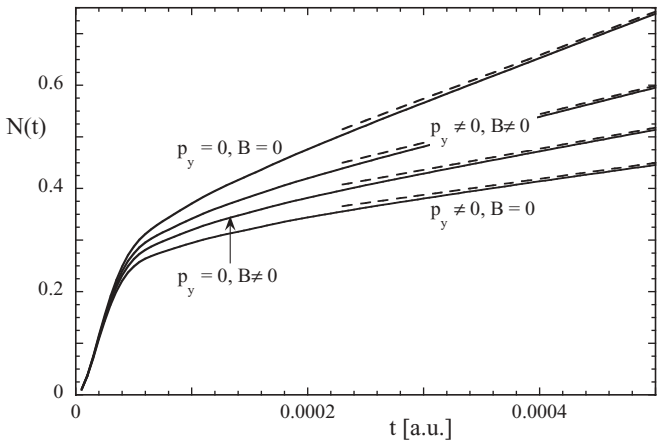

FIG. 2. The number of created pairs as a function of time for $W = 0.1/c$, $V = 2.5c^2$, and $M = 0.6c^2$. In the long-time limit, the curves approach straight lines with slopes of 843.93, 553.71, 407.75, and 310.45, respectively. These slopes are computed analytically in Sec. VI. The two curves labeled $p_y \neq 0$ correspond to the simulations with $p_y = -62.83$.

We next examine the corresponding electron spatial distributions. They are displayed in Fig. 3 with identical parameters as used in Fig. 2. Both static electric and magnetic fields are centered at $x = 0$ with a width of $W = 0.1/c = 0.00073$ a.u. corresponding to a narrow range around the origin. Since the barrier is repulsive on the right side for the electron, the electron moves to the left and the positron (not shown in Fig. 3) moves to the right. At time $t = 0.0005$ the initially created electrons have moved mostly to the left and the wave front reached to around $x = 0.07$ a.u. This corresponds to an effective traveling speed of $v = 0.07/0.0005 \sim 137 = c$.

The electrons, when being created, have roughly the same probability of traveling to the left and to the right. The portion that travels to the left will continue to travel to the left. Outside of the interaction region the electron undergoes a free evolution with possible quantum spreading.

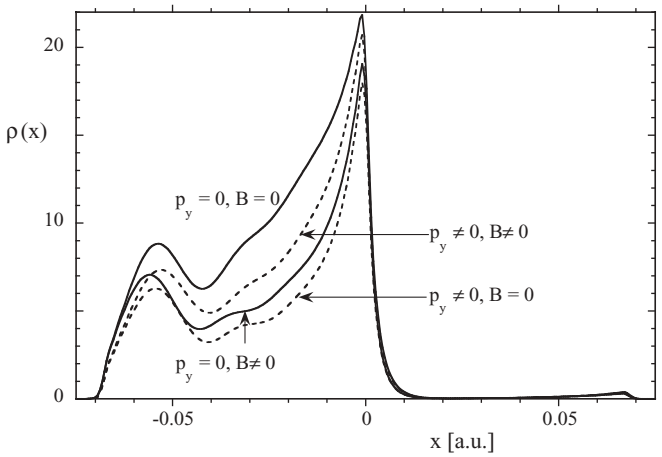

FIG. 3. The spatial distribution for the created electrons for $W = 0.1/c$, $V = 2.5c^2$, and $M = 0.6c^2$ at time $t = 0.0005$. The solid curves are for $p_y = 0$, the dashed curves are for $p_y = -62.83$. The case of a static electric field is labled with $B = 0$ while the case of combined **E** and **B** fields is labled with $B \neq 0$.

The portion of the electron that travels to the right can be divided into two groups. Most electrons have an energy that is below the maximum barrier height so after climbing the barrier they come to rest before they slide down the potential to escape to the left to minus infinity. A small number of electrons have an energy that is larger than the maximum barrier height. These electrons can manage to overshoot the barrier and move to the right. The small peak on the right of the origin in Fig. 3 represents the electron that has undergone this type of motion. The small peak near $x = 0.07$ a.u. is due to the sudden turn on of the electric fields and thus a slightly higher density is formed as a "wave front." The fastest velocity of the right moving electrons is also near the speed of light. The higher density for the electrons that eventually move to the left near $x = -0.055$ is also due to the sudden turn on.

The overall height of each curve in Fig. 3 is consistent with Fig. 2. In fact, for $p_y = 0$ the B field suppresses the pair creation but for $p_y \neq 0$ the effect can also be an *enhancement*. There are several structures in the spatial density distributions, which depend on the particular value of p_y.

B. For momentum $p_y \neq 0$

For the case of $p_y \neq 0$ at an instant t, the evolution can be chosen as

$$\psi_n^{p_y}(x,y,t) = e^{ip_y y}\,\zeta_n^{p_y}(x,t_0)\,. \tag{5.2}$$

Because of momentum p_y conservation, only the matrix elements with the same p_y are nonzero. In this case the Hamiltonian is

$$h = c\alpha_x \hat{p}_x + c\alpha_y p_y + \alpha_y A_y(x) + \beta c^2 + V(x). \tag{5.3}$$

The total number of electrons with a fixed momentum p_y can be calculated similar to those for $p_y = 0$. The resulting time-dependent pair creation signal and the spatial density distributions are similar to those associated with $p_y = 0$. The corresponding pair creation was shown in Fig. 2 and the spatial distributions were shown in Fig. 3 with the label $p_y \neq 0$. In our example, p_y has been assumed to be -62.83. This particular value was chosen to illustrate that the pair creation for some p_y can be enhanced. In our numerical calculations the momentum takes only discrete values. The specific value quoted above ($\sim 100\ 2\pi$) is just the result of our chosen parameters for the numerical grid. While the data for $p_y = -62.83$ and $p_y = 0$ are quite similar, we notice that the suppression obtained early can be reversed into an enhancement. In other words, for $p_y = -62.83$ the pair creation in the presence of magnetic field is enhanced (instead of suppressed) compared to the case of $p_y = 0$.

C. Total pair creation and the corresponding spatial density

In order to compute the total pair creation and the corresponding spatial density we need to add up the individual contributions associated with each values of p_y. Our set of (uncoupled) 1D equations is then identical to a single 2D calculation.

The result of the total pair creation is displayed in Fig. 4 and the corresponding spatial distribution is shown in Fig. 5.

Even though for some values of p_y the presence of the magnetic field enhances and some other values suppress the

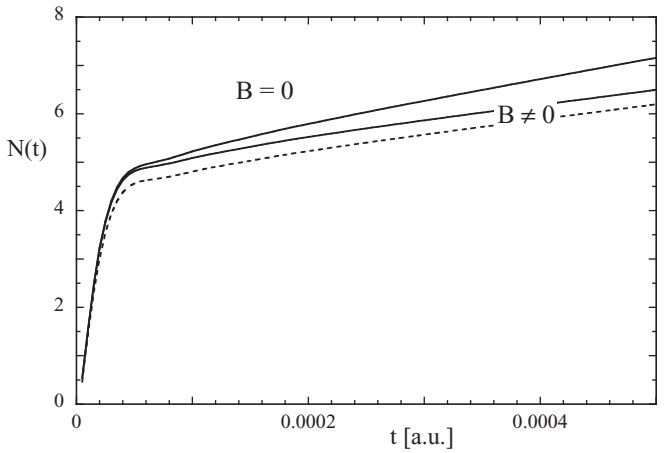

FIG. 4. The total number of the created electrons as a function of time t. $W = 0.1/c$, $V = 2.5c^2$ (top solid line), and additionally $M = 0.6c^2$ (lower solid line). The slopes in the long-time limit for the top and the lower solid curves are 4312.2 and 3004.2, respectively. The dashed curve is for $M = 0.6c^2$ also and is explained in Sec. VI. It has essentially the same long-time limit slope as the lower solid curve.

pair creation, the number of total pairs is always suppressed in the presence of the magnetic field. This conclusion is obvious from Figs. 4 and 5.

From Fig. 4 we also see that the pair creation increases from zero as the electric field is switched on at $t = 0$. For short times of $1/c^2$, it grows independent of the magnetic field strength. In the long-time limit it approaches linear regions that can be represented by a constant slope, which represents the creation rate. These rates can be computed also by other means, as we show in Sec. VI. In the long-time limit our numerical result approaches the computed rate extremely well. The curves with the magnetic field show a significant amount of suppression of pair creation compared to the pure static electric field case. This result with nonzero magnetic field is interesting. Unlike the case when the static E field is parallel to the B field [12,14] for which the pair creation is believed to be slightly enhanced by the magnetic field, the configuration with

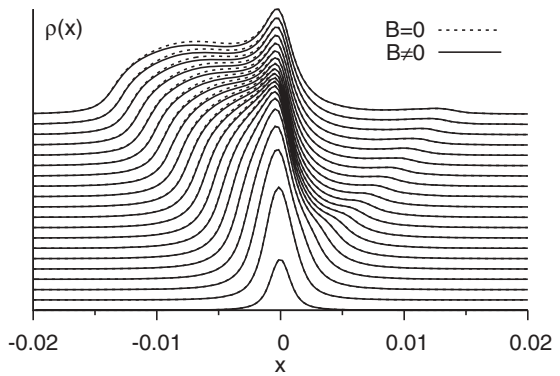

FIG. 5. Snapshots of the electron densities at time $t_n = n \times 5 \times 10^{-5}$ a.u. ($n = 1, 2, \ldots, 20$). The dashed curves are for the case of a static electric field only, while the solid curves are for the case of combined **E** and **B** fields with the same parameters as in the Fig. 4. For better visibility, we have added a constant vertical shift to each distribution to represent the time evolution.

the E field perpendicular to the B field produces an overall suppression of created pairs.

There are several ways to explain how the magnetic field might suppress the pair creation. For example, we could consider transforming the observer to a moving frame in which the magnetic field is completely absent. It turns out that in this moving frame the effective electric field strength is lower than its original value. Since the pair creation is, in general, proportional to the amplitude of the electric field the observed suppression of pair creation due to the magnetic field is obvious.

We could also argue that the presence of the magnetic field causes the created electrons to execute a quasicircular cyclotron motion. Such a motion can return the electron back to the interaction zone where the pair creation occurs. The returned electron can occupy the same state a newly created electron would require. Due to the Pauli exclusion principle for fermions, the pair creation is suppressed. Note the suppression presented in Fig. 4 can be seen most prominently after the early stage of $t \sim 0.000\,05$, similar to the starting time of suppression in Fig. 2.

The suppression obviously manifests itself also in the spatial domain, as shown in Fig. 5. In this plot we see that the electrons created at $x = 0$ moved away from the interaction region. The speed of the electrons is close to the speed of light. The small density in the opposite direction corresponds to high-momentum electrons that could climb over the potential barrier. Outside of the field region it just moves with a uniform speed, which happens to be very close to the speed of light again. Since the probability of overcoming the barrier is small, the resulting spatial density is small. Note that there are certain momentum values that correspond to the electrons moving up the potential barrier initially but eventually do not overcome the barrier. These electrons will reverse their motion to move away from the barrier. They will register on the same side as those that were created and moved down the barrier and away from the barrier. Note that the cyclotron radius of the created electron in this case should be around $0.25/c$ for our simulation parameters. After adding all p_y up, the density in Fig. 5 is very smooth when compared to Fig. 3.

VI. LONG-TIME BEHAVIOR OF THE PAIR CREATION

A. Creation rate and its relation to the transmission coefficient

We observed from the previous discussions that in the long-time limit the creation curves settle into a straight line. This means that the process in the long-time limit can be approximated by a single rate that corresponds to the slope of the line. In order to analyze the pair creation rate and its variation with energy, we study the transmission of a particle moving from a positive energy state to a negative state in a supercritical barrier. In one spatial dimension one can show that the long-time limits of the pair-creation rate can be obtained from the energy integral over the transmission coefficient as [30,37,46]

$$S = \frac{1}{2\pi}\int_{c^2}^{V-c^2} T(E)dE. \tag{6.1}$$

The key question is how well this well-known relationship between quantum mechanical single-particle scattering and pair creation also holds if in addition a magnetic field is present.

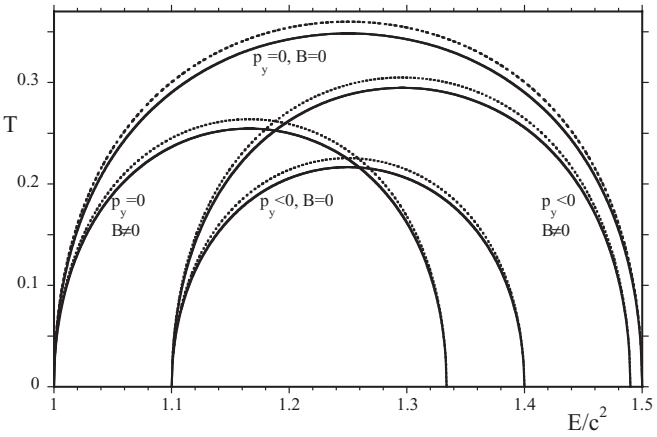

FIG. 6. The quantum mechanical transmission coefficient T as a function of incoming energy E. For all cases $V = 2.5c^2$, $W = 0.1/c$. For $B \neq 0$, $M = 0.6c^2$. For fixed nonzero momentum $p_y = -62.83$. The dash curves are the analytical results for the step potential case from Eq. (C9).

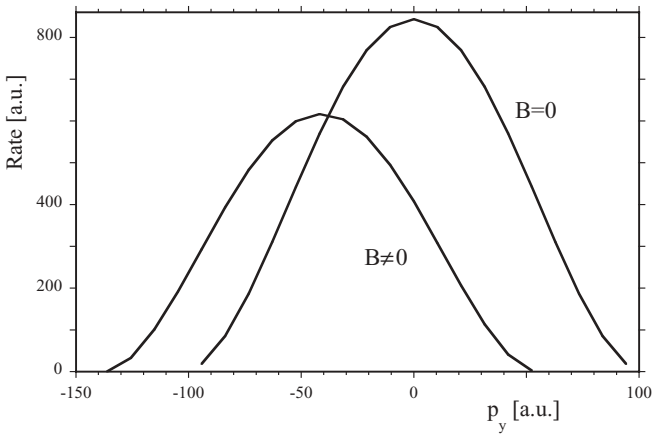

FIG. 7. The pair creation rate R for various p_y, with and without magnetic field. $V = 2.5c^2$, $M = 0.6c^2$, and $W = 0.1/c$.

For a specific momentum p_y, we generalize this formula to

$$S(p_y) = \frac{1}{2\pi}\int_{E_{\min}}^{E_{\max}} T_{p_y}(E)dE \tag{6.2}$$

where $E_{\min} = \sqrt{[c^4 + c^2 {p_y}^2]}$ and $E_{\max} = V - \sqrt{[c^4 + c^2(p_y + M/c)^2]}$. This generalization ensures the energy of integration for the states is within the Klein region. If we add all $S(p_y)$ including the spin we obtain for the total rate $S = 2\sum_{p_y} S(p_y)$. In the general case, transmission coefficient T can be obtained numerically through single-particle evolution or by the quantum transmitting boundary method (QTBM; see Appendix B). The numerical results with $p_y = 0$ for static **E** field or static **E** and **B** fields are illuminated in Fig. 6.

The area from Fig. 6 times 2 (spin, assumed four spinor components in our calculations) fits the slope in Fig. 2. As a matter of fact, the four slope values that the curves approached in the long-time limit came from an evaluation of the corresponding areas of the semicircled structures in Fig. 6. The agreement with the numerical result is excellent and confirms the validity of Eq. (6.1) even for the more general case of a magnetic field. For example, the numerical slopes in Fig. 2 of 857.11, 563.14, 415.20, and 317.07 differ from the computed rates by only 1.6%, 1.7%, 1.8%, and 2.1%, respectively. It is quite interesting to find that Eq. (6.1) is valid even for combined electric and magnetic fields. Of course, the transmission only requires us to solve the single particle scattering problem. This agreement shows once again a mathematical connection between QFT and (single-particle) quantum mechanics.

Note that there is a constraint on the parameters V and M. The supercritical threshold corresponds to $V > 2c^2$ for a static electric field. Here the overlap between the negative and positive energy states leads to the following inequality, $E_{\max} > E_{\min}$ or $V - \sqrt{[c^4 + c^2(p_y + M/c)^2]} > \sqrt{[c^4 + c^2 {p_y}^2]}$. This inequality simplifies to $V^2 - M^2 > 4c^4$ if p_y is zero. Otherwise, no positive states can transmit into the negative states; thus, no permanent flux of electron-positron pairs can occur. This is consistent with an argument for **E** and **B** fields described above based on Lorentz boosted frame, where there is only an effective static electric field. Here the amplitude of the effective scalar potential is given by $\sqrt{[V^2 - M^2]}$ such that in this frame the condition for supercriticality translates into $\sqrt{[V^2 - M^2]} > 2c^2$.

B. Variation of pair creation rate with momentum p_y

We have compared the rates using the formulas developed in Sec. VIA with the numerical simulations presented in Sec. V. In Fig. 7 we show how the pair creation rate varies with the value of p_y with and without magnetic field. This figure also explains why for $p_y = 0$ there is a suppression due to the B field and for $p_y = -62.83$ there is an enhancement as displayed in Figs. 2 and 4. This is quite interesting as this dependence on p_y is not monotonic. In fact, there is an apparent shift in the peak value to the left in Fig. 7 with the increase of the magnetic field. Also there is an apparent suppression in the overall area that, after multiplied by $L_y/(2\pi)$, corresponds to half of the slopes in Fig. 4 (the factor of 2 accounts for the spin).

For the case of $M = 0$, a nonzero p_y has two effects on the pair creation rate in Eq. (6.1). It leads to a higher limit for $E_{\min}$ and a lower limit for $E_{\max}$ compared to the case of $p_y = 0$. For example, for $p_y = -62.83$ the lowest energy one can obtain is $\sqrt{[c^4 + c^2 {p_y}^2]}$. This explains why the corresponding curves in Fig. 6 did not begin from the origin. We also note from the analytical results for the extreme narrow field (see Appendix C) that p_y causes a mass shift from m (1 in a.u.) to a larger effective mass according to $m^* = \sqrt{[m^2 + (p_y/c)^2]}$ that enters the expression of transmission coefficient T. Thus, we can expect a maximum value for $p_y = 0$.

When $M \neq 0$, as A_y and V have the same spatial configuration, one can introduce a Lorentz transformation along the y axis

$$\begin{pmatrix} ct' \\ x' \\ y' \\ z' \end{pmatrix} = \begin{pmatrix} \gamma & 0 & -\beta\gamma & 0 \\ 0 & 1 & 0 & 0 \\ -\beta\gamma & 0 & \gamma & 0 \\ 0 & 0 & 0 & 1 \end{pmatrix} \begin{pmatrix} ct \\ x \\ y \\ z \end{pmatrix}. \tag{6.3}$$

With $\beta = v/c = -A_y/V = -M/V_0 = -0.6/2.5 = -0.24$ and $\gamma = 1/\sqrt{[1 - \beta^2]} = 1.03$. After this transformation, the new fields are $A'_y = \gamma(\beta V + A_y) = 0$ and $V' = \gamma(V + \beta A_y) =$

$\sqrt{[V_0{}^2 - M^2]}\,[1 + \tanh(x/W)]/2$. Thus, in the new inertial frame, the field is again a pure electric field with the same spatial configuration but with the lower potential $V_0' = \sqrt{[V_0{}^2 - M^2]}$. The most probable energy and longitude momentum in this frame of reference for the created electron is $E' = V_0'/2$ and $p_y' = 0$. This corresponds to the largest transmission coefficient. Thus, the peak value shifts to $p_y = -M/2c$ due to the existence of a magnetic field. When we transform back to the original frame of reference we obtain $p_y = \gamma p_y' + \gamma E'\,\beta/c = -M/2c = -0.6c2\ /2/c = -0.3c = -41.11$. From Fig. 7 the peak is roughly located at -41.89, so the error is around only 2%. Because of the reduction of the effective potential, the peak value for the pair creation has to be suppressed. The most probable energy in the former frame of reference is $E = \gamma E' + c\gamma\beta p_y' = V_0/2$.

To see how our simple Lorentz transformation-based analysis is valid for our situation, we have made a simulation for $V = 2.5c^2$, $M = 0.6c^2$ and where the pair creation has been obtained by an integration over all momenta p_y. The pair creation agrees with $V' = \sqrt{(V^2 - M^2)} = 2.427c^2$ $M' = 0$ case. The predicted creation rates are 3.14×10^3 and 3.13×10^3, respectively; that is, they differ by less than 0.4%. This is the origin of the dashed curve in Fig. 4. The slope for the long-time limit is nearly identical to that of the lower solid line. However, different short-time behaviors give rise to the shift between the two curves.

In Fig. 6 we can see the curves take elliptical shapes, and the area under the curve is the rate in Fig. 7. To approximate the semicircle by an ellipse introduces an error on the order of 3% to 4% for the area. The energy integration in the integral over the transmission rate ranges from $E_{\min} = \sqrt{[c^4 + c^2 p_y{}^2]}$ to $E_{\max} = V - \sqrt{[c^4 + c^2(p_y + M/c)^2]}$. We can therefore choose the half of the energy interval $\Delta E = (E_{\max} - E_{\min})/2$ and the relevant transmission rate $T(E_{\rm pr})$ as the semimajor and the semiminor axis of the ellipse, respectively. Here $E_{\rm pr}$, which equals $(E_{\max} - E_{\min})/2 + E_{\min,}$ is the most probable energy and the value of $T(E_{\rm pr})$ can be obtained from Eq. (C9). The center of the ellipse is at the point $(E_{\rm pr}, 0)$.

This rate is half of the area, namely $R = S/2 = \Delta E\, T(E_{\rm pr})/2$. Therefore, we get the ratio of the rate with and without the magnetic field: $R|_{B=0}/R|_{B\neq 0} = (\Delta E\, T(E_{\rm pr}))|_{B=0}/(\Delta E\, T(E_{\rm pr}))|_{B\neq 0}$. In our situation, we get $R|_{B=0,\,p_y=-62.83}/R|_{B\neq 0,\,p_y=-62.83} = 0.568$, and $R|_{B\neq 0,\,p_y=0}/R|_{B=0,\,p_y=0} = 0.489$. They agree excellently with a small error of less than 2% with the ratios of the slopes shown in Fig. 2, $310.45/553.71 = 0.561$ and $407.75/843.93 = 0.483$. When the momentum is integrated out, $R_{\rm tot} = \frac{L_y}{2\pi}\int_{p_{\min}}^{p_{\max}} \frac{\Delta E\, T(E_{\rm pr})}{2} dp_y$, we obtain the estimated total rate of pair creation to be 3041.85 (for $B \neq 0$) and 4350.42 (for $B = 0$). Comparing with the slopes obtained from Fig. 4, 3004.2 (for $B \neq 0$) and 4312.2 (for $B = 0$), the error is again very small and under 2%.

C. The constant field limit

The pair creation rate per unit volume per unit time for mutually perpendicular static and spatially homogeneous EM fields [14,40] is (again in atomic units) for the 2D system

$$R_s = \frac{\varepsilon^{3/2}}{2\pi^2 c^{1/2}} \exp\left(-\frac{\pi c^3}{\varepsilon}\right), \tag{6.4}$$

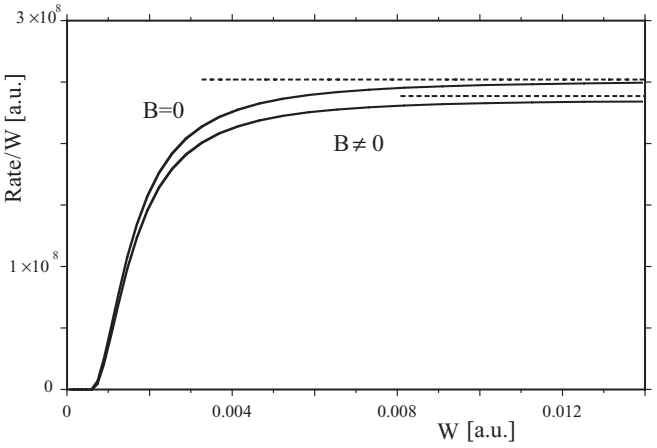

FIG. 8. The pair creation rate as a function of the field's width W. The two dashed lines are calculated from Eq. (6.4) after integration over x and y. The solid curves are calculated from Eq. (6.2) after integration over all p_y. [$V_0 = 25c^3$ W and $M = 6c^3$ W]

where $\varepsilon = \sqrt{[E^2 - B^2]}$. Within the locally constant field approximation and integration over space we can compute the total number of created pairs. The results are shown in Fig. 8. For field widths W much greater than the Compton wavelength $1/c$, the locally constant field approximation gives a nearly perfect description of the pair creation rates. However, for widths W within the Compton wavelength, this approximation leads to deviations from the exact results. When $W < 6 \times 10^{-4}$, the exact pair creation rate is zero, which corresponds to a subcritical potential $V_0 < 2c^2$.

VII. DISCUSSION AND OUTLOOK

In summary, we have examined the electron-positron pair creation for a configuration, where the electric and magnetic fields are perpendicular to each other. We further allowed both fields to have a spatial dependence in one direction permitting us to study for the first time the effect of a localized interaction region with full spatial and temporal resolution. It permits us to examine the dynamics by computing the short- and long-time evolution of the spatial particle density. These simulations extend prior findings (for spatially uniform fields) where one can compare the usual Schwinger pair creation rate with a modified one for the long-time limit. In agreement with these findings we observe that the magnetic field can severely suppress the creation process. The time-resolved analysis of the spatial density permits us to illustrate the underlying physical mechanisms. These space-time resolved studies become computationally feasible, as the field configuration can be reduced to a set of 1D problems.

For differently aligned electric and magnetic fields that are also inhomogeneous in space and time it is presently not possible to simulate the pair-creation process in full space-time resolution. The required fully 3D simulation is computationally very demanding and one has to rely on different techniques. For example, it is not clear what happens when the electric field and magnetic fields are parallel to one another. Early work based on the long-time rates for spatially and temporally homogeneous fields suggest a possible weak

enhancement of the pair creation rate, but any physical mechanism that could explain this is presently lacking. It is also not clear how this suggestion needs to be modified to account for the unavoidable spatial inhomogeneities.

It seems that the effect of the magnetic field on the pair creation dynamics is rather sensitive to the mutual angle between both fields and only the two extreme cases of precisely parallel or perpendicular alignments have been studied systematically. It would be interesting to learn what happens when the two fields are neither exactly perpendicular nor parallel. There could be an interesting middle point where the suppression associated with perpendicular arrangement and the enhancement associated with the parallel arrangement could compete directly with each other.

In this study we have assumed for simplicity that the spatial inhomogeneities of the electric and magnetic field are identical. Our numerical simulation technique would permit us also to explore how the more general case where the two fields only overlap partially or have different widths. We will devote separate works to these important issues.

ACKNOWLEDGMENTS

We enjoyed several helpful discussions with Dr. B. Galow, Dr. K. Hatsagortsyan, Dr. Y. T. Li, Dr. X. Lu, S. Meuren, Dr. A. Milstein, Dr. C. Müller, Dr. A. Di Piazza, Dr. R. Wagner, and Dr. J. Zhang. This work has been supported by the NSF and the NSFC (Grant No. 11128409). R.G. acknowledges the kind hospitality of MPIK during his sabbatical leave. Q.S. acknowledges the kind hospitality offered by the CAS during his sabbatical leave where the project was initiated.

APPENDIX A: THE EQUIVALENCE OF THE A AND V GAUGES IN STATIC ELECTRIC FIELDS

For a 1D system without a magnetic field, the equivalence for the pair creation between the A gauge (with $V = 0$) and the V gauge (with $\mathbf{A} = 0$) can be easily proven. In the V gauge, the pair creation is determined by the matrix element $U^{\mathrm{V}}{}_{p,n} \equiv \langle p|U^{\mathrm{V}}|n\rangle$, where p and n denote the positive and negative eigenstates of the free Hamiltonian h_0 and U^{V} is the time evolution operator in the V gauge. We denote the result in the V gauge by a superscript V and the A gauge by a superscript A. One can go from the V gauge to the A gauge via the transformations

$$V'(x) = V(x) - \frac{1}{c}\frac{\partial}{\partial t}\chi\,(x,t) = 0, \tag{A1a}$$

$$A_x\,(x,t) = \frac{\partial}{\partial x}\chi\,(x,t)\,. \tag{A1b}$$

The choice of $\chi(x,\,t)$ is not unique, and we can always choose a transform such that $A(x,t=0) = 0$. In such a case $h^{\mathrm{A}}(t_0) = h_0$, the eigenstates for $h^{\mathrm{A}}(t_0)$ are just the field-free p, n states as mentioned before. From the gauge invariance of the Dirac equation, the field-free states $|n\rangle$ evolve with time in the A gauge according to

$$|\phi_n\,(t)\rangle = \exp\left[-i\,\chi\,(x,t)\,/c\right]U^{\mathrm{V}}\,|n\rangle\,. \tag{A2}$$

On the other hand, one can show that

$$\begin{aligned}
&h^{\mathrm{A}}(t)\exp\left[-i\,\chi\,(x,t)\,/c\right]|\,p\rangle\\
&\quad=\left[c\alpha_x p_x+\alpha_x A_x\,(x,t)+\beta c^2\right]\exp\left[-i\,\chi\,(x,t)\,/c\right]|\,p\rangle\\
&\quad=\exp\left[-i\,\chi\,(x,t)\,/c\right]h_0\,|p\rangle+c\alpha_x\,|p\rangle\left(-i\frac{\partial}{\partial x}\right)\\
&\qquad\times\exp\left[-i\,\chi\,(x,t)\,/c\right]+\alpha_x A_x\,(x,t)\\
&\qquad\times\exp\left[-i\,\chi\,(x,t)\,/c\right]|\,p\rangle\\
&\quad=\left\{E_p+\alpha_x\left[A_x\,(x,t)-\frac{\partial}{\partial x}\chi\,(x,t)\right]\right\}\\
&\qquad\times\exp\left[-i\,\chi\,(x,t)\,/c\right]|\,p\rangle\\
&\quad=E_p\,\exp\left[-i\,\chi\,(x,t)\,/c\right]|\,p\rangle\,.
\end{aligned} \tag{A3}$$

In other worlds, $\exp[-i\,\chi(x,t)/c]|p\rangle$ is a eigenstate of $h^{\mathrm{A}}(t)$ at every instant time t with energy $E_p = \sqrt{c^4 + c^2p^2}$. There is an obvious gap between the positive and negative states. The orthonormality relation is preserved. For example, $\langle p'|\exp[i\,\chi(x)t/c]\exp[-i\,\chi(x)t/c]|p\rangle = \langle p'|p\rangle$.

In conclusion, we find that $|\,\psi_{\mathcal{P}}\rangle = \exp\left[-i\,\chi(x)t/c\right]\,|\,p\rangle$ and $|\,\psi_{\mathcal{N}}\rangle = \exp\left[-i\,\chi(x)t/c\right]\,|n\rangle$, which satisfy $h^{\mathrm{A}}(t)|\,\psi_{\mathcal{P}}\rangle = E_p|\,\psi_{\mathcal{P}}\rangle$ and $h^{\mathrm{A}}(t)|\,\psi_{\mathcal{N}}\rangle = E_n|\,\psi_{\mathcal{N}}\rangle$, form a complete set at every instant t for the Hamiltonian $h^{\mathrm{A}}(t)$ in the A gauge. Because of the gap between $E_p = \sqrt{c^4 + c^2p^2}$ and $E_n = -\sqrt{c^4 + c^2p^2}$, there exists a gap between the positive and negative states at every instant t. As a result we can write

$$\begin{aligned}
U^{\mathrm{A}}_{\mathcal{P},n} &= \langle\psi_{\mathcal{P}}\,|\,\phi_n(t)\rangle\\
&= \langle p\,|\exp\left[i\,\chi(x)t/c\right]\exp\left[-i\,\chi(x)t/c\right]U^{\mathrm{V}}|\,n\rangle = U^{\mathrm{V}}_{p,n}.
\end{aligned} \tag{A4}$$

The equivalence holds also for the other matrix element in Eq. (3.5).

Next we provide some simulation results to illustrate the equivalence between the A and the V gauge in a static electric field. For the pair creation in the A gauge, the system is described by a static electric field with the gauge $A_z = A_y = V = 0$, and

$$A_x(x) = \frac{cV_0\,(t-0.0003)}{2W}[1-\tanh^2(x/W)]. \tag{A5}$$

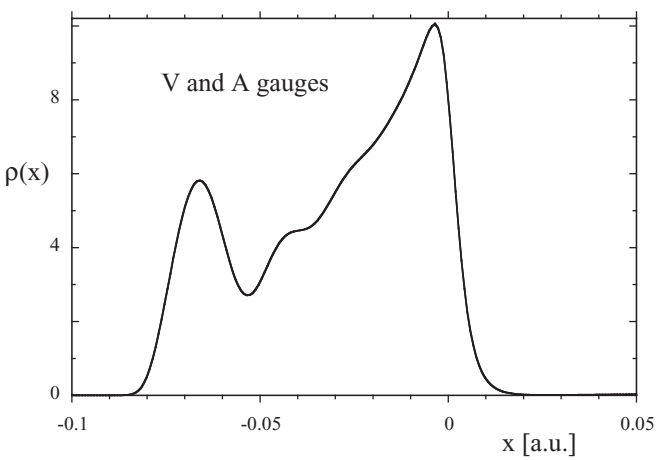

FIG. 9. Comparison of the electric density created by A and V at $t = 0.0006$, $V = 2.53c^2$, $W = 0.5/c$.

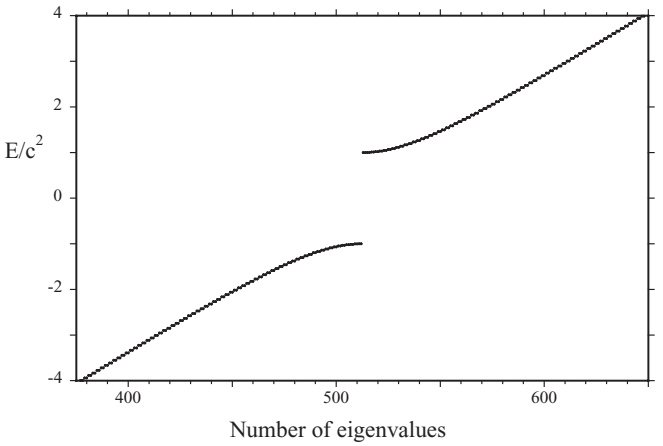

FIG. 10. The energy eigenvalues for the Hamiltonian in A gauge at $t = 0$ and $t = 0.0006$. Same parameters as Fig. 9 are used.

For the V gauge, $A_x = A_y = A_z = 0$, and

$$V(x) = V_0/2\,[1 + \tanh(x/W)]\,. \tag{A6}$$

Figure 9 is the probability density obtained with the V and the A gauges, respectively. The results are identical. Figure 10 is the energy spectrum of the states in the A gauge when the field is supercritical, the gap between the positive and negative energy states is obvious.

APPENDIX B: THE QUANTUM TRANSMITTING BOUNDARY METHOD FOR DIRAC EQUATION

The scattering of a single particle described by the Dirac equation for a field defined by the scalar and the vector potentials $V(x)$ and $\mathbf{A}(x)$ can be discussed within the framework of the so-called QTBM. For simplicity, let us consider the case when the potentials vary only along the x direction and are constant for $x \leqslant 0$ and $x \geqslant 0$. In the Klein region, the general solution to Dirac's equation $\psi(x)$ in these regions can be written as

$$\psi(x) = \begin{cases} a_0 e^{ip_x x + ip_y y}/\sqrt{2\pi} + b_0 e^{-ip_x x + ip_y y}/\sqrt{2\pi}, & x < 0, \\ c_0 e^{-iq_x x + ip_y y}/\sqrt{2\pi}, & x > 0, \end{cases} \tag{B1}$$

where the spinors take the form

$$a_0 = \frac{1}{\sqrt{2E}} \begin{pmatrix} \sqrt{E + c^2} \\ 0 \\ 0 \\ \frac{cp_x + icp_y}{cp}\sqrt{E + c^2} \end{pmatrix},$$

$$b_0 = \frac{r}{\sqrt{2E}} \begin{pmatrix} \sqrt{E + c^2} \\ 0 \\ 0 \\ \frac{-cp_x + icp_y}{cp}\sqrt{E + c^2} \end{pmatrix}, \tag{B2}$$

$$c_0 = \frac{t\,|\mathcal{J}|}{\sqrt{2E'}} \begin{pmatrix} \sqrt{E' - c^2} \\ 0 \\ 0 \\ \frac{cq_x - i(cp_y + M)}{cq}\sqrt{E' + c^2} \end{pmatrix},$$

and where $E' = V - E$, $E' = \sqrt{[c^4 + c^2 q^2]}$, $q = \sqrt{[{q_x}^2 + (p_y + M/c)^2]}$, and the Jacobian $|\mathcal{J}| = |\frac{dE}{dp_x}/\frac{dE'}{dq_x}| = E'_{px}/E_{qx}$. The Hamiltonian reads

$$h(x) = \begin{pmatrix} c^2 + V(x) & 0 & 0 & c\hat{p}_x - i[cp_y + A_y(x)] \\ 0 & c^2 + V(x) & c\hat{p}_x + i[cp_y + A_y(x)] & 0 \\ 0 & c\hat{p}_x - i[cp_y + A_y(x)] & -c^2 + V(x) & 0 \\ c\hat{p}_x + i[cp_y + A_y(x)] & 0 & 0 & -c^2 + V(x) \end{pmatrix}. \tag{B3}$$

If we discretize the operator $\hat{p}_x$ such that $\hat{p}_x f_j = -i\,\partial f_j/\partial x = -i(f_j - f_{j-1})/\Delta_x = -i(f_{j+1} - f_j)/\Delta_x$. The discrete form of the Dirac equation, $h\psi = E\psi$, then becomes

$$(c^2 + V_j)\Delta_x \psi_j^1 - ic\left(\psi_j^4 - \psi_{j-1}^4\right) - i(cp_y + A_{yj})\Delta_x \psi_j^4 = E\Delta_x \psi_j^1 \tag{B4a}$$

$$-ic\left(\psi_{j+1}^1 - \psi_j^1\right) + i(cp_y + A_{yj})\Delta_x \psi_j^1 + (-c^2 + V_j)\Delta_x \psi_j^4 = E\Delta_x \psi_j^4. \tag{B4b}$$

To obtain the QTBM equations, we need to solve the equations on the boundary by adding points at $j = 0$ and $j = n + 1$:

$$a_1 = \varepsilon_1 \psi_0^4 + \chi_1 \psi_1^1, \tag{B5a}$$

$$a_n = \varepsilon_n \psi_{n+1}^1 + \chi_n \psi_n^4. \tag{B5b}$$

Using Eq. (B1) on the boundary points we get a set of solution

$$\varepsilon_1 = (p_x + ip_y)/\sqrt{E - c^2}$$
$$\chi_1 = e^{ip_x \Delta_x}/\sqrt{E + c^2}$$
$$a_1 = [(p_x + ip_y)e^{-ip_x \Delta_x}/(p_x - ip_y) + e^{ip_x \Delta_x}]e^{ip_x x_1}/\sqrt{2E} \tag{B6a}$$

and

$$\begin{aligned}\varepsilon_n &= e^{iq_x\Delta_x}/\sqrt{E'-c^2}\\ \chi_n &= -[cq_x + i(cp_y + M)]/cq\sqrt{E'+c^2}.\\ a_n &= 0\end{aligned} \tag{B6b}$$

Adding Eqs. (B6a) and (B6b), the discrete Dirac equation has the matrix representation

$$\begin{bmatrix} \varepsilon_1 & \chi_1 & & & & \\ s_1 & d_1 & u_1 & & & \\ & S_1 & D_1 & U_1 & & \\ & & \ddots & \ddots & \ddots & \\ & & & S_n & D_n & U_n \\ & & & & \chi_n & \varepsilon_n \end{bmatrix} \begin{bmatrix} \psi_0^4 \\ \psi_1^1 \\ \psi_1^4 \\ \vdots \\ \psi_n^4 \\ \psi_{n+1}^1 \end{bmatrix} = \begin{bmatrix} a_1 \\ 0 \\ 0 \\ \vdots \\ 0 \\ a_n \end{bmatrix}, \tag{B7}$$

where $d_j = (c^2 + V_j - E)\,\Delta_x$, $s_j = ic$, $u_j = -ic - i(cp_y + A_{yj})\Delta_x$, $D_j = (-c^2 + V_j - E)\,\Delta_x$, $S_j = ic + i(cp_y + A_{yj})\Delta_x$, and $U_j = -ic$.

APPENDIX C: SCATTERING OF A PARTICLE WITH A FINITE p_y WITH A STEP POTENTIAL

For a supercritical step potential barrier with $V > 2c^2$ and a step potential with A_y, the transmission coefficient T can be obtained analytically. We investigate the 2D scattering process in a potential $V(x)$ combined with a step vector potential $A_y(x)$ which is independent of y and z. The potentials may be expressed as $V(x) = \frac{V}{2}[1 + \theta(x)]$ and $A_y(x) = \frac{M}{2}[1 + \theta(x)]$. Note $\theta(x) = -1$ for $x < 0$ and $\theta(x) = 1$ for $x \geqslant 0$. The Hamiltonian reads

$$h = c\alpha_x\hat{p}_x + c\alpha_y\hat{p}_y + \alpha_y A_y(x) + \beta c^2 + V(x). \tag{C1}$$

This is the Hamiltonian for the case of $p_z = 0$. In the region $x < 0$, the incoming wave can be chosen as

$$\Psi_I^+ = \frac{1}{\sqrt{2E}} \begin{pmatrix} \sqrt{E+c^2} \\ 0 \\ 0 \\ \frac{cp_x + icp_y}{cp}\sqrt{E+c^2} \end{pmatrix} \frac{e^{ip_x x + ip_y y}}{2\pi} \tag{C2a}$$

or

$$\Psi_I^- = \frac{1}{\sqrt{2E}} \begin{pmatrix} 0 \\ \sqrt{E+c^2} \\ \frac{cp_x - icp_y}{cp}\sqrt{E-c^2} \\ 0 \end{pmatrix} \frac{e^{ip_x x + ip_y y}}{2\pi}. \tag{C2b}$$

The reflected wave is

$$\Psi_R^+ = \frac{r}{\sqrt{2E}} \begin{pmatrix} \sqrt{E+c^2} \\ 0 \\ 0 \\ -\frac{cp_x - icp_y}{cp}\sqrt{E-c^2} \end{pmatrix} \frac{e^{-ip_x x + ip_y y}}{2\pi} \tag{C3a}$$

or

$$\Psi_R^- = \frac{r}{\sqrt{2E}} \begin{pmatrix} 0 \\ \sqrt{E+c^2} \\ -\frac{cp_x + icp_y}{cp}\sqrt{E-c^2} \\ 0 \end{pmatrix} \frac{e^{-ip_x x + ip_y y}}{2\pi}, \tag{C3b}$$

where $E = \sqrt{c^4 + c^2p^2}$, $p^2 = p_x^2 + p_y^2$, with $c^2 < E < V - c^2$. The transmitted wave is

$$\Psi_T^+ = \frac{t\,|\mathcal{J}|}{\sqrt{2E'}} \begin{pmatrix} \sqrt{E'-c^2} \\ 0 \\ 0 \\ \frac{cq_x - i(cp_y + M)}{cq}\sqrt{E'+c^2} \end{pmatrix} \frac{e^{-iq_x x + ip_y y}}{2\pi} \tag{C4a}$$

or

$$\Psi_T^- = \frac{t\,|\mathcal{J}|}{\sqrt{2E'}} \begin{pmatrix} 0 \\ \sqrt{E'-c^2} \\ \frac{cq_x + i(cp_y + M)}{cq}\sqrt{E'+c^2} \\ 0 \end{pmatrix} \frac{e^{-iq_x x + ip_y y}}{2\pi}. \tag{C4b}$$

The superscripts + and − in Eqs. (C2a) to (C4b) denote the two different spins. In the following calculations, our results are the same for either kind of spin. Here $E' = V - E$, $E' = \sqrt{[c^4 + c^2q^2]}$, $q = \sqrt{[q_x{}^2 + (p_y + M/c)^2]}$. The Jacobian $|\mathcal{J}| = |\frac{dE}{dp_x}/\frac{dE'}{dq_x}| = E'p_x/Eq_x$. Since this is an energy eigenstate we have $h\psi = E\psi$. The continuum condition at $x = 0$ leads to a set of equations:

$$1 + r = t\frac{\sqrt{E}}{\sqrt{E'}}\,|\mathcal{J}|\,\mu, \tag{C5a}$$

$$\begin{aligned}&\frac{cp_x \pm icp_y}{cp} - \frac{cp_x \mp icp_y}{cp}r\\ &\quad= t\frac{\sqrt{E}}{\sqrt{E'}}\,|\mathcal{J}|\,\nu\frac{cq_x \mp i(cp_y + M)}{cq},\end{aligned} \tag{C5b}$$

where $\mu = \frac{\sqrt{E'-c^2}}{\sqrt{E+c^2}}$, $\nu = \frac{\sqrt{E'+c^2}}{\sqrt{E-c^2}}$. Substituting $(cp_x - icp_y)/cp$ with a, the condition $T + R = 1$ ($R = |r|^2$, $T = |t|^2|\mathcal{J}|$) as

$$\begin{aligned}1 - R &= \frac{p}{p_x}\mathrm{Re}[(1 + r)(a - a^*r^*)]\\ &= tt^*|\mathcal{J}||\mathcal{J}|\mu\nu\frac{pq_xE}{p_xqE'} = T.\end{aligned} \tag{C6}$$

The equation above can be further simplified by substitutions

$$\begin{aligned}b &= \frac{cq_x - i(cp_y + M)}{cq}, \quad j = t\frac{\sqrt{E}}{\sqrt{E'}}\,|\mathcal{J}|\,,\\ 1 + r &= j\mu, \quad a^* - ar = jvb,\\ a^* + a &= j\,(a\mu + bv) = 2p_x/p.\end{aligned} \tag{C7}$$

Note:

$$\begin{aligned} jj^* &= \frac{4p_x^2}{p^2}\frac{1}{(a\mu+b\nu)(a^*\mu+b^*\nu)} \\ &= \frac{4p_x^2}{p^2}\frac{1}{\mu^2+\nu^2+\mu\nu(ab^*+a^*b)} \\ &= \frac{2p_x^2}{p^2}\frac{c^2p^2}{E'E+c^4+cp_xcq_x+cp_y(cp_y+M)}. \end{aligned} \tag{C8}$$

We finally arrive at

$$T = \frac{jj^*q_x}{p_x} = \frac{2c^2p_xq_x}{E'E+c^4+cp_xcq_x+c^2p_y(p_y+M/c)}. \tag{C9}$$

The magnetic field dependence is described by the terms $(p_y + M/c)$ and E' in the transmitted part. Note that for $M = 0$ the transmission reduces to

$$T = \frac{2c^2p_xq_x}{E'E+c^4+cp_xcq_x+c^2p_y^2}. \tag{C10}$$

If we restore the mass m in the expression (again in atomic units, $m = 1$ is assumed), the longitudinal momentum p_y adds only an additional term to the mass m compared to the case of $p_y = 0$. The efficient mass $m*$ then satisfies $m^{*2}c^4 = m^2c^4 + c^2{p_y}^2$. An effective mass increase is apparent from this expression when $p_y \neq 0$.

[1] O. Klein, Z. Phys. **53**, 157 (1929).
[2] F. Sauter, Z. Phys. **69**, 742 (1931).
[3] J. S. Schwinger, Phys. Rev. **82**, 664 (1951).
[4] A. Hansen and F. Ravndal, Phys. Scr. **23**, 1036 (1981).
[5] B. R. Holstein, Am. J. Phys. **66**, 507 (1998).
[6] B. R. Holstein, Am. J. Phys. **67**, 499 (1999).
[7] G. V. Dunne, Q. H. Wang, H. Gies, and C. Schubert, Phys. Rev. D **73**, 065028 (2006); D. D. Dietrich and G. V. Dunne, J. Phys. A **40**, F825 (2007).
[8] G. V. Dunne and C. Schubert, Phys. Rev. D **72**, 105004 (2005).
[9] H. Gies and K. Klingmüller, Phys. Rev. D **72**, 065001 (2005).
[10] S. Kim and D. Page, Phys. Rev. D **65**, 105002 (2002).
[11] E. S. Fradkin, D. M. Gitman, and Sh. M. Shvartsman, *Quantum Electrodynamics with Unstable Vacuum* (Springer, Berlin, 1991); for some exact solvable examples, see V. G. Bagrov and D. M. Gitman, *Exact Solutions of Relativistic Wave Equations* (Kluwer Academic, Netherlands, 1990).
[12] N. Tanji, Ann. Phys. (Leipzeg) **324**, 1691 (2009).
[13] N. B. Narozhnyi and A. I. Nikishov, Sov. J. Nucl. Phys. **11**, 596 (1970); A. I. Nikishov, Sov. Phys. JETP **30**, 660 (1970).
[14] Qiong-gui Lin, J. Phys. G: Nucl. Part. Phys. **25**, 17 (1999).
[15] A. Di Piazza and G. Calucci, Phys. Rev. D **65**, 125019 (2002); Astropart. Phys. **24**, 520 (2006).
[16] D. L. Burke *et al.*, Phys. Rev. Lett. **79**, 1626 (1997).
[17] H. Hu, C. Müller and C. H. Keitel, Phys. Rev. Lett. **105**, 080401 (2010).
[18] A. Di Piazza, E. Lötstedt, A. I. Milstein, and C. H. Keitel, Phys. Rev. Lett. **103**, 170403 (2009).
[19] A. Di Piazza, A. I. Milstein, and C. H. Keitel, Phys. Rev. A **82**, 062110 (2010).
[20] N. B. Narozhny, S. S. Bulanov, V. D. Mur, and V. S. Popov, JETP **102**, 9 (2006); Phys. Rev. Lett. **104**, 220404 (2010).
[21] V. S. Popov, JETP Lett. **13**, 185 (1971).
[22] C. Müller, A. B. Voitkiv, and N. Grün, Phys. Rev. Lett. **91**, 223601 (2003); Phys. Rev. A **67**, 063407 (2003); **70**, 023412 (2004).
[23] C. Deneke and C. Müller, Phys. Rev. A **78**, 033431 (2008); C. Müller, C. Deneke, and C. H. Keitel, Phys. Rev. Lett. **101**, 060402 (2008).
[24] P. Sieczka, K. Krajewska, J. Z. Kamiński, P. Panek, and F. Ehlotzky, Phys. Rev. A **73**, 053409 (2006); J. Z. Kamiński, K. Krajewska, and F. Ehlotzky, *ibid.* **74**, 033402 (2006); K. Krajewska and J. Z. Kamiński, *ibid.* **82**, 013420 (2010); **84**, 033416 (2011).
[25] V. S. Popov, JETP Lett. **74**, 133 (2001); V. S. Popov, Phys. Lett. A **298**, 83 (2002).
[26] A. Di Piazza, Phys. Rev. D **70**, 053013 (2004).
[27] G. V. Dunne, H. Gies, and R. Schützhold, Phys. Rev. D **80**, 111301 (R) (2009).
[28] R. Schützhold, H. Gies, and G. Dunne, Phys. Rev. Lett. **101**, 130404 (2008).
[29] M. Jiang, W. Su, Z. Q. Lv, X. Lu, Y. J. Li, R. Grobe, and Q. Su, Phys. Rev. A **85**, 033408 (2012).
[30] G. R. Mocken, M. Ruf, C. Müller, and C. H. Keitel, Phys. Rev. A **81**, 022122 (2010).
[31] T. Cheng, S. P. Bowen, C. C. Gerry, Q. Su, and R. Grobe, Phys. Rev. A **77**, 032106 (2008).
[32] A. Ringwald, Phys. Lett. B **510**, 107 (2001).
[33] R. Alkofer *et al.*, Phys. Rev. Lett. **87**, 193902 (2001); C. D. Roberts, S. M. Schmidt, and D. V. Vinnik, *ibid.* **89**, 153901 (2002).
[34] M. Ruf, G. Mocken, C. Müller, K. Z. Hatsagortsyan, and C. H. Keitel, Phys. Rev. Lett. **102**, 080402 (2009).
[35] M. Tatarakis, I. Watts, F. N. Beg, E. L. Clark, A. E. Dangor, A. Gopal, M. G. Haines, P. A. Norreys, U. Wagner, M.-S. Wei, M. Zepf, and K. Krushelnick, Nature (London) **415**, 280 (2002).
[36] A. Pukhov and J. Meyer-ter-Vehn, Phys. Rev. Lett. **76**, 3975 (1996).
[37] T. Cheng, M. R. Ware, Q. Su, and R. Grobe, Phys. Rev. A **80**, 062105 (2009).
[38] P. Krekora, Q. Su, and R. Grobe, Phys. Rev. Lett. **92**, 040406 (2004).
[39] P. Krekora, K. Cooley, Q. Su, and R. Grobe, Phys. Rev. Lett. **95**, 070403 (2005).
[40] T. Cheng, Q. Su, and R. Grobe, Phys. Rev. A **80**, 013410 (2009).
[41] W. Greiner, B. Müller, and J. Rafelski, *Quantum Electrodynamics of Strong Fields* (Springer-Verlag, Berlin, 1985).

[42] G. A. Mourou, T. Tajima, and S. V. Bulanov, Rev. Mod. Phys. **78**, 309 (2006).
[43] A. I. Akhiezer and R. V. Polovin, Sov. Phys. JETP **30**, 915 (1956).
[44] J. W. Braun, Q. Su, and R. Grobe, Phys. Rev. A **59**, 604 (1999).
[45] G. R. Mocken and C. H. Keitel, Comp. Phys. Comm. **178**, 868 (2008).
[46] M. Jiang, W. Su, X. Lu, Z. M. Sheng, Y. T. Li, Y. J. Li, J. Zhang, R. Grobe, and Q. Su, Phys. Rev. A **83**, 053402 (2011).